# Digital Discovery

## PAPER

Check for updates

# SALSA: a low-cost self-driving lab modular add-on for salt solubility assessment for battery electrolytes

Tianyi Zhang, [ID] †[a] Hongyi Lin, [ID] †[a] Yuhan Chen [ID] [b] and Venkatasubramanian Viswanathan [ID] *[ab]

Solubility is the maximum amount of solutes that can dissolve in a certain amount of solvent at a certain temperature, and it is significant in battery electrolyte research since it confines the design space. Thus, solubility measurement is a critical constraint on running self-driving labs for battery electrolyte design. Herein, we introduce a low-cost experiment-execution and decision-making level Self-Driving Lab (SDL) modular add-on for automated solubility measurement of liquid electrolytes, enabling automated liquid dosing, powder dosing, weighing, stirring, temperature tracking, and dissolution recognition process *via* Python control, which plays a crucial role in accelerating electrolyte discovery and optimization. This solubility testing add-on module costs around 100 US dollar to build (in addition to the system previously built in our research group), gains good performance against benchmark data, and collects new solubility results of sodium bis(fluorosulfonyl)imide (NaFSI) salt in pure and mixed solvents of acetonitrile (ACN), 1,2-dimethoxyethane (DME), and ethyl methyl carbonate (EMC) under tracked room temperature of 25.4 ± 0.2 °C.

## 1 Introduction

Batteries are electrochemical devices that store and convert chemical energy into electrical energy through redox reactions, making them essential for a wide range of applications, from consumer electronics to electric vehicles and grid storage.[1] In essence, a battery consists of three primary components: the anode, the cathode, and the electrolyte. The electrolyte, a crucial component, facilitates the movement of ions between the electrodes during its operation.[2] The performance and longevity of a battery are highly dependent on the electrolyte's ionic conductivity, electrochemical stability, and interfacial compatibility with electrode materials.[3] As battery research progresses, innovations in electrolyte formulations continue to play a pivotal role in enhancing battery performance, lifespan, and safety.[4]

One critical aspect of battery electrolyte design criteria is salt solubility, which directly influences ion transport, electrochemical stability, and overall battery performance. In high-concentration electrolytes, solubility becomes particularly crucial, as it dictates the maximum achievable ion concentration, which in turn affects ionic conductivity and

electrochemical behavior.[5] Unlike conventional dilute electrolytes, where ions are freely solvated, highly concentrated electrolytes form unique solvation structures that can enhance electrochemical stability, suppress solvent decomposition, and improve interfacial compatibility with electrodes.[6] However, poor solubility at high concentrations can lead to salt precipitation, increased viscosity, and hindered ion mobility, ultimately limiting battery performance.[7] Achieving an optimal balance between stability and transport properties is essential for the development of next-generation batteries, particularly for next-generation alkali metal battery systems, where electrolyte stability and ion transport efficiency play a pivotal role in long-term cycling and safety.[8]

Despite the significance of solubility in battery electrolytes, the traditional way of manually measuring solubility is time consuming and prone to human errors.[9,10] These limitations have motivated growing interest in automated and data-driven experimental paradigms. In this context, Reber *et al.* highlighted the need for robotically automated solubility measurement systems as a critical step toward overcoming the inefficiency and variability of conventional techniques.[11] This perspective aligns with the broader emergence of Self-Driving Laboratories (SDLs), which couple automated experimentation with artificial intelligence (AI)-guided decision making to accelerate scientific discovery.[12] Currently multiple SDLs have been built for a variety of applications.[13–18] Yik *et al.* developed ODACell, an automated; robotic setup capable of coin cell assembly and electrolyte formulation,[19] Oh *et al.* developed

*a*Department of Mechanical Engineering, University of Michigan, Ann Arbor, MI, 48105, USA. E-mail: tiz@umich.edu; lithium@umich.edu

*b*Department of Aerospace Engineering, University of Michigan, Ann Arbor, MI, 48105, USA. E-mail: cyhalek@umich.edu; venkvis@umich.edu

† Equal contribution.

Electrolab, a commercial 3D printer adapted SDL for automated characterization of redoxactive electrolytes,[20] MacLeod et al. developed Ada, a SDL capable of autonomously synthesizing, processing, and characterizing organic thin films commonly used in perovskite solar cells and consumer electronics,[21] Fisker-Bødker et al. developed AMPERE-2, a robotic platform for automated electrodeposition and electrochemical validation,[22] and Wang et al. developed NIPS, a fully automated platform for fabrication and characterization of porous polymeric membranes.

This work builds upon Clio, an automated non-aqueous liquid electrolyte testing system capable of density, conductivity, and viscosity measurement.[23] Clio functions in a way that saturated solutions with salt dissolved in solvent at the highest possible concentration are pre-made manually, thereby allowing built-in algorithms to make desired solutions with concentration below or equal to solubility. However, since available resources provide experimental salt solubility data for a limited range of non-aqueous electrolytes[24] and rigorous solubility calculation is computationally demanding,[25] often times solutions need to be manually prepared iteratively to find the concentration upper bound, which is time-consuming. To address this problem, in this work, coupled with the valves, pumps, and balance previously installed in Clio, an automated solubility screening platform is built.

For solubility measurements, two main approaches are commonly used: the excess solid method and the excess solvent method.[26] In the excess solid method, solute is gradually added to a fixed volume of solvent until undissolved solids appear, producing high-quality data but requiring time-consuming analytical techniques such as high-performance liquid chromatography (HPLC),[27,28] which slows down the workflow and contradicts with the high throughput purpose. By contrast, the excess solvent method incrementally adds solvent to a fixed amount of solute until complete dissolution is achieved. Shiri et al. demonstrated a fully automated closed-loop robotic platform for the excess solvent method, integrating both solid and liquid handling to achieve high-precision results.[29] Shiri et al.'s work does set a great example of automated solubility measurement in general chemical discovery, but there was no such platform designed specifically for battery electrolyte research. Also, their system relies on a high-precision robotic arm and an automated solid doser. Both devices are prohibitively expensive, with costs in the tens of thousands of US dollars. Since precise automated solid dosing is typically more technically challenging and costly than automated liquid dosing,[30] we developed a low-cost solid doser based on a 3D-printed Archimedes screw.

The Archimedes screw is a widely adopted solution for solid dispensing in industrial systems, including those offered by suppliers such as Sirius Automation, demonstrating its reliability and suitability for controlled solid handling.[31] Implementing 3D printing to this mechanism not only reduces expenses but also promotes innovation by enabling researchers to share, modify and improve existing designs.[32]

Within the platform, this solid doser is tightly integrated into the autonomous solubility workflow, as it directly interfaces with the motors and relays already deployed in the Clio system. Together with a highly precise yet affordable peristaltic pump for liquid handling, this integrated solid–liquid dosing configuration provides a cost-effective and scalable solution for automated solubility experiments.

Meanwhile, classifying dissolution status is another critical component of solubility measurement. Shiri et al. proposed a functional solution for this task: firstly identifying the vial within the image, and then determining the dissolution status by analyzing turbidity over time.[29] While effective, this method requires reference images, region of interest selection and repeated image analysis over extended periods, causing intensified complexity, reduced flexibility, and increased runtime. Therefore, a classification model made with YOLO (You Only Look Once), a real time object detection algorithm,[33] is developed for determining the dissolution status. The model also uses a two-step pipeline: using computer vision algorithm to first locate the vial, and then directly classify the dissolution status with only one image through YOLO model. This approach increases the simplicity, flexibility, and efficiency of the pipeline.

In this paper, inspired by Shiri et al.'s work, we introduced the first automated solubility measurement system in the field of battery electrolyte research using a novel Archimedes screw-based automated solid dosing system and a computer vision algorithm for dissolution detection. Given the fact that high-precision automated solid dosing is generally more costly and challenging than high-precision automated liquid dosing,[34] SALSA (SALt Solubility Assessment) implements the excess solvent method to facilitate high-throughput salt solubility analysis using liq-uid handling and weighing systems developed in our previous work.[23] The system is first validated against established bench-mark solubility data of sodium nitrate ($NaNO_3$) and lithium sulfate ($Li_2SO_4$) in DI water respectively. Then, it is used to collect new solubility data for sodium salts, specifically sodium bis(fluorosulfonyl)imide (NaFSI) in both pure and mixtures of non-aqueous solvents of acetonitrile (ACN), dimethyl ether (DME), and ethyl methyl carbonate (EMC).

## 2 Experimental

### 2.1 Hardware pipeline

The 3D CAD design figure of the whole platform is shown in Fig. 1, and this platform is fully controlled by our Python-based GUI system, ElyteOS,[35] and consists of: (a) liquid transfer, (b) solid transfer, (c) stirring, (d) dissolution recognition, and (e) temperature tracking as in Fig. 2.

The system initiates operation by dispensing at least a predetermined amount of 0.3 g solid via the auto-solid doser. The doser is fabricated in a way that a motor is attached to a 3D printed Archimedes screw, and the screw is placed inside a y-shaped 3D printed polylactic acid (PLA) tube with one end storing solid and the other end rotating the screw to dispense solid. And for the mass, it is read from the balance placed below the vial holder and uses closed-loop mass feedback. The balance has a highly precise resolution of 0.1 mg and the
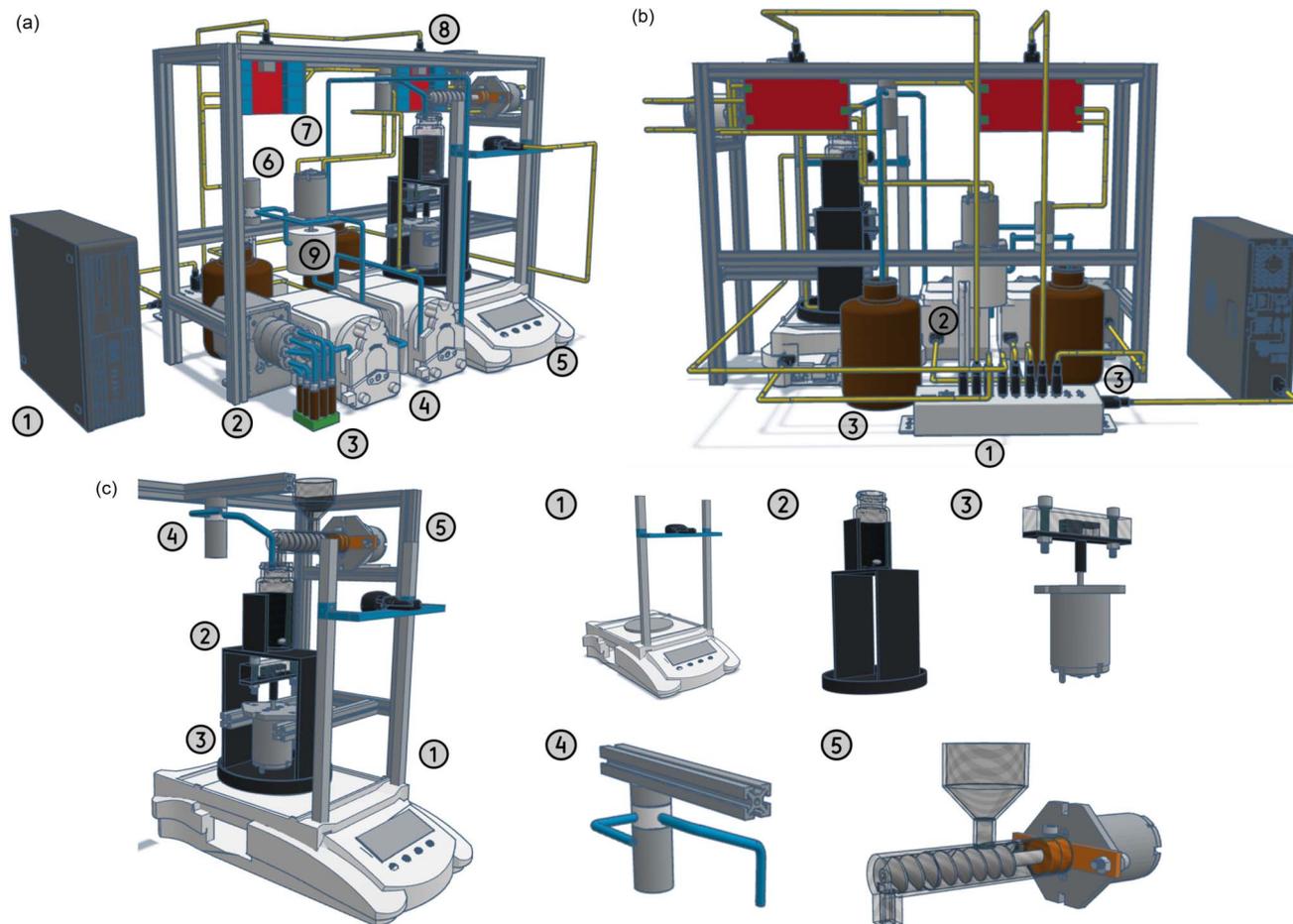
Fig. 1 (a) Front-left view: (1) desktop, (2) 10-port valve, (3) 9 vials containing feeder solvents, (4) peristaltic pumps, (5) integrated weighing, liquid dosing, solid dosing system (breakdowns explained in (c)), (6) 3-way valve, (7) 24V USB relay controlling 3-way valves, (8) 12V USB relay controlling DC motors. (b) Back view: (1) USB dock, (2) USB thermometer, (3) waste tanks. (c) Breakdown of (5) in (a): (1) balance and webcam, (2) 3D printed vial holder and vial with magnetic stir bar inside, (3) magnetic stirrer consisting of a 12V DC motor and a 3D printed mounting with magnetic bars inside, (4) 3-way valve connected with liquid tubes, (5) 12V motor, 3D printed Archimedes screw, and 3D printed tube with funnel. Note: yellow tubes indicate wires connecting electronic devices and blue tubes indicate tubes transferring liquid(s).

reading is only considered stable after 15 consecutive identical readings.

Once the salt is in place in the vial, the pump will dispense a predetermined 0.5 mL liquid(s) of the desired concentration(s) from the 10-port valve that is connected to the feeding solvents. The Python controllable peristaltic pump used is Longer L100-1S-2, and it is capable of accurately dispensing liquid of a given volume.

After both solid and liquid are transported into the container, the stirrer, made from a 3D printed stirrer rod attached to a 12V motor, will facilitate the mixing of the solutions. During the mix-ing process, the webcam integrated with computer vision algorithm captures the predetermined region of the vial and determines whether the solute is dissolved or not based on whether the turbidity is stable over time.

If the computer vision algorithm determines that the salt is fully dissolved, the mass of solute and the volume of solvent will be recorded to calculate the solubility. If not, solvent will be added stepwise at an increment of 0.1 mL per step at a rate of 5 mL per minute along with a 2.5 s predetermined equilibrium period and iteratively until salt dissolution is detected or the maximum volume of the vial is reached. And if the maximum volume is reached, SALSA will report a solubility lower than a lower-bound solubility estimate based on the amount of salt and solvents added till this point.

Since solubility is inherently temperature-dependent, a thermometer was placed adjacent to the vial holder, measuring and tracking ambient temperature near the solution throughout the entire experiment.

Alongside with the main pipeline, careful cleaning, flushing, and drying procedures are carried out to ensure electrolyte purity. After each experiment, the solution will be manually dumped into the waste tank and rinsed with DI water. After that, all used vials will be put into the vacuum oven overnight before returning to use.

## 2.2 Computer vision algorithm

The dissolution status of the solution was determined using computer vision algorithms. Images were acquired *via* a webcam positioned approximately 20 cm from the vial, with the
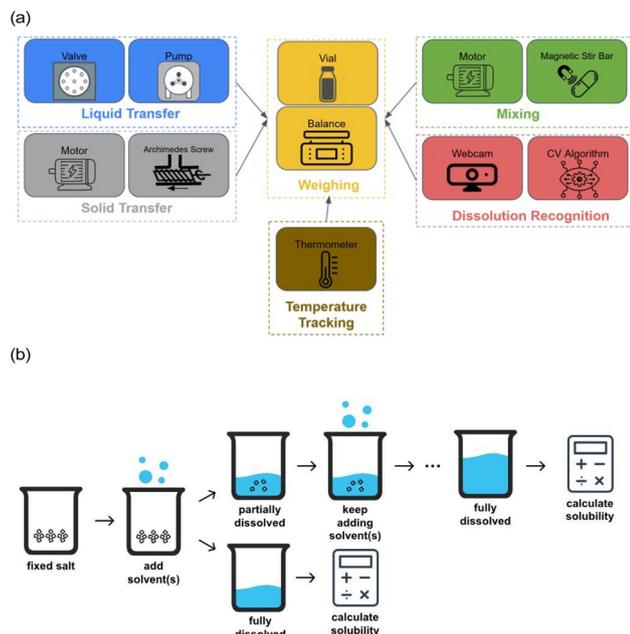
Fig. 2 (a) Overall structure: valves and pumps transfer the liquid to the vial while the motor attached to the Archimedes screw dispenses solid to the flask, with weight measured by the balance below the vial. The motor attached to the stirrer stirs the mixture while the webcam integrated with computer vision algorithm detects whether the salt is dissolved or not. Throughout the process, the temperature is tracked using a thermometer. (b) Excess solvent method: solvent is added stepwise to a solute until a fully dissolved state is observed to calculate solubility.

focus value optimized to 55 cm (Fig. S5) and LED light as light source attached directly on top of the webcam. Inspired by the Hein-sight framework,[29] a two-stage pipeline was implemented: first, a YOLO detection model was applied to localize the vial; subsequently, a YOLO classification model was used to assess the dissolution status. YOLO was selected due to its efficiency—processing each image in a single pass[33]—and its robust performance on small datasets enabled by transfer learning.[36] Unlike turbidity sensors that might better suit well-defined solvent systems, computer vision enables discrimination between multiple dissolution-relevant states, including undissolved solids settled at the bottom, transient clouding during mixing, bubble formation, and wall adhesion artifacts, which are difficult to distinguish using single-channel turbidity measurements. Also, turbidity thresholds are highly solvent and path-length dependent, requiring recalibration for each solvent system. In contrast, CV enables qualitative dissolution state recognition without assuming a linear optical response. Therefore, in this scenario, vision-based approaches offer greater flexibility for heterogeneous workflows.

Two image classes were defined for model training: "clear" (DI water) and "sediment" (liquid containing visible undissolved $NaNO_3$ or NaFSI). Representative examples are shown in Fig. S4 and S16, and the dataset distribution is summarized in Table S4. The detection model parameters are provided in Table S2, with corresponding results shown in Fig. S6–S12. Similarly,

the classification model parameters are listed in Table S3, with results presented in Fig. S13–S15.

During classification, an image was captured and evaluated following each round of liquid addition. The process continued irrespective of the interim results. A solution was considered fully dissolved only when the model predicted "clear" in three consecutive classifications; any "sediment" prediction reset this count.

## 3 Results and discussion

Our solubility screening platform integrates a computer vision algorithm with a modular hardware system to enable automated solubility measurements using the excess solvent method. Clear and sediment images were collected to train and validate the CV model, while benchmark solubility data from publicly available chemical databases were used for cross-validation prior to generating new experimental datasets.

Fig. 4 presents the performance of the CV model in classifying clear and sediment states. The model achieved 100%
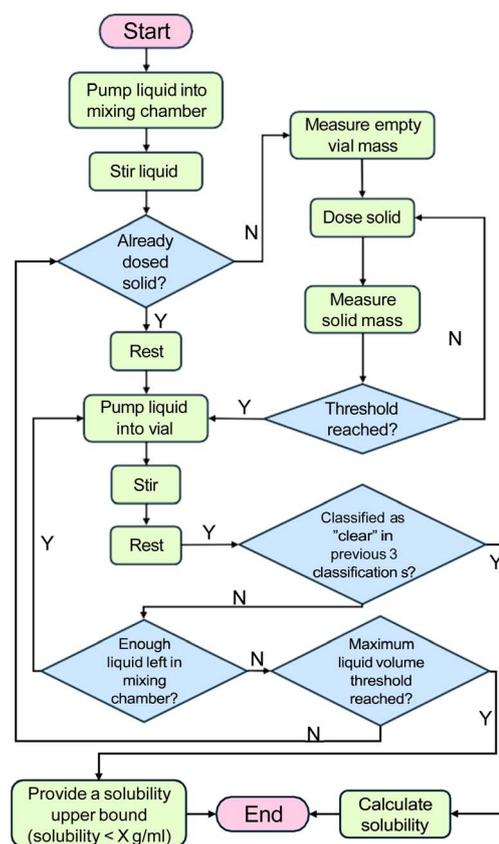


Fig. 3 Workflow: (a) for each run, solid is transferred into the vial first, then the solvent is dosed next. (b) Mix the solid and liquid mixture. (c) Use the camera integrated with computer vision algorithm to determine dissolution. (d) If dissolved, calculate the solubility. If not, iterate the process to add solvent stepwise till complete dissolution is observed or the maximum volume of the vial is reached. (e) If the maximum liquid volume threshold of the vial is reached without full dissolution, the system outputs a lower-bound solubility estimate (solubility < X).
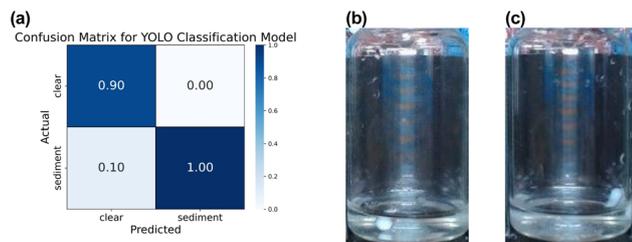
Fig. 4 (a) Confusion matrix of the YOLO classification model on the validation dataset. (b) A boundary solution classified as "clear". (c) A boundary solution classified as "sediment".

accuracy when identifying the sediment state and 90% accuracy when identifying the clear state. While the latter reflects strong overall performance, occasional misclassifications of the clear state may undermine the reliability of solubility assessments. To mitigate this issue, a stricter classification protocol was implemented, requiring three consecutive clear predictions before confirming a fully dissolved state, as illustrated in Fig. 3. This refinement substantially reduces the likelihood of false positives in practice and enhances the robustness of automated solubility determinations in downstream analyses.

We next validated the accuracy of solubility measurements using two salts with distinct solid-flow properties: coarse-grained, less viscous $NaNO_3$, and fine-powder, more viscous $Li_2SO_4$, both dissolved in DI water. To accommodate their different dosing behaviors, two customized solid-doser heads were designed as in S1 of SI file: a standard funnel for $NaNO_3$ and a wider-neck, shorter-exit funnel for $Li_2SO_4$ to mitigate clogging and ensure smoother powder flow. Due to the more coarse particle size distribution, and less flowability behavior, which affect screw-based dosing reproducibility, it leads to the higher variability observed for $NaNO_3$ as shown in S2 of SI. And specifically in the context of battery electrolyte research, since the set of salts commonly explored is relatively limited compared to the number of possible solvents, these salts are generally well characterized in terms of their physical handling behavior and SALSA currently assumes a prior knowledge of material handling requirements.

As shown in Fig. 5, the solubility values obtained with SALSA fell within 20% of benchmark values from PubChem[37] and Chemical Book,[38] which is a significant improvement over conventional simulation discrepancies that often exceed 50%. Although a 20% deviation remains relatively high, this error primarily arises from several inherent system limitations, including less precise control of solid dispensing and temperature, uncertainty in CV-based phase classification near saturation, calibration drift in the pump and balance, rapid solvent-addition rate, and short equilibration time. Nevertheless, the results demonstrate SALSA's capability to reliably characterize known salts. Moreover, in battery electrolyte research, relative solubility trends across different solvent compositions are often more critical than exact absolute values. From this perspective, SALSA's primary contribution lies in automating labor-intensive experimental workflows and enabling high-throughput
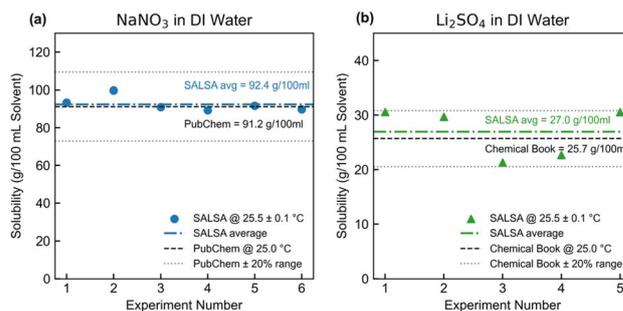


Fig. 5 (a) $NaNO_3$ and (b) $Li_2SO_4$ solubility in DI Water (in g/100 mL of solvent) validation against benchmark results in PubChem and Chemical Book.

solubility trend mapping at scale, rather than replacing high-accuracy analytical instrumentation.

Building on these benchmarks, we further explored new solubility measurements of NaFSI salt in both pure and mixed non-aqueous solvents, including ACN, DME, and EMC. Fig. 6 shows subtle interplay for multi-component solvents where we considered two cases, both with DME as the base solvent and adding ACN and EMC. At 50 : 50 ratio, we observe both negative and positive excess solubility, showing that SALSA is capable of generating consistent and chemically meaningful solubility data across multi-solvent systems, providing a foundation for mapping complex electrolyte–solvent interactions relevant to battery research.

In Fig. 6, the concentration unit "M" denotes an approximated molarity, defined as moles of salt per liter of the final solution under the assumption of ideal volume additivity. Specifically, the salt mass measured by the balance was converted to moles using its known molar mass, while the solution volume was calculated summing up the dispensed solvent(s) volume and the calculated salt volume based on its density. This approximation avoids direct density measurement of the final solution while maintaining internal consistency for comparative analysis.

In summary, our results demonstrate that the integration of CV-based classification model with modular solid-dosing hardware enables reproducible and flexible solubility measurements of a given salt across different solvent compositions and formulations. While limitations of current restriction to single-salt systems, lack of precise control on solid dispensing and temperature, rapid solvent-addition rate, short
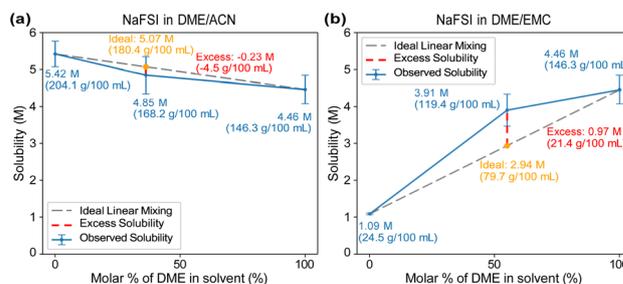


Fig. 6 Solubility (in M) with error bar *v.s.* solvent molar percentage in solvents (in %) (a) NaFSI in ACN/DME (b) NaFSI in DME/EMC.

equilibration time, the assumption of prior knowledge of salt flowing properties, and the need to manually clean and dry vials after the experiments and manually replace dosing heads when switching materials remain, SALSA represents a step toward more autonomous self-driving laboratories. Future work will focus on enabling multi known and unknown salt solubility measurements under improved solid dispensing and temperature control, further refining CV-based classification strategies for higher accuracy, and a greater level of autonomy.

# 4 Conclusions

In this work, we introduced SALSA, a low-cost experiment-execution and decision-making level self-driving laboratory modular add-on for automated salt solubility assessment in battery electrolytes. The platform enables automated, high-throughput solubility measurements at a material and financial cost orders of magnitude lower than conventional robotic systems, and we include a comparison table comparing accuracy, throughput and initial cost among SALSA, Shiri *et al.*, and manual measurement in the SI. Validation against benchmark data confirmed the accuracy of the approach, while new measurements in pure and mixed non-aqueous solvents demonstrate the platform's ability to generate previously unavailable datasets critical for electrolyte design.

The combination of modular hardware and CV-based dissolution recognition highlights how inexpensive automation can accelerate electrolyte discovery, streamline iteration cycles, and expand accessible chemical design space. More importantly, the critical data delivered lowers the barrier for broad adoption across academic and industrial research groups.

But still, some limitations remain: the current implementation, based on the excess solvent method, is best suited to single known salt systems and lacks precise control over dispensed solid mass with the observation that the doser has better control on fine-powder, more cohesive salt. Future development could focus on interchangeable multi-doser arrays and the development of a more universal doser head designed to robustly handle a wider range of powder morphologies and flow characteristics. Additionally, the use of a basic webcam and non-optimized illumination constrains robustness across different vial geometries, solvents, and lighting conditions, and determining whether a training image represents a fully dissolved or undissolved sample can be subjective, introducing potential variability in the dataset. Future development could incorporate higher-quality optical sensing techniques or hybrid optics–computer vision approaches under controlled lighting to more objectively identify dissolution states.

Overall, SALSA represents a step toward democratizing self-driving labs by providing a scalable, adaptable, and affordable tool for electrolyte salt solubility measurement, which is essential for advancing next-generation batteries.

# Author contributions

Tianyi Zhang: formal analysis, investigation, methodology, project administration, validation, visualization, writing – original draft. Hongyi Lin: conceptualization, investigation, methodology, project administration, writing – original draft. Yuhan Chen: formal analysis, data curation, investigation, methodology, software, writing – original draft. Venkatasubramanian Viswanathan: conceptualization, funding acquisition, supervision, writing – review & editing. All authors have reviewed and approved the final version of the manuscript.

# Conflicts of interest

There are no conflicts to declare.

# Data availability

All the code, data, 3D printing CAD files, and additional results associated with this work can be found at https://github.com/BattModels/SALSA (DOI: https://doi.org/10.5281/zenodo.18987462) and supplementary information (SI). Supplementary information: detailed hardware design, bills of materials, as well as model architectures, training parameters, representative datasets, and performance metrics for the computer vision-based solubility classification workflow. See DOI: https://doi.org/10.1039/d5dd00516g.

# Acknowledgements

# Notes and references

1 J. B. Goodenough and K.-S. Park, *J. Am. Chem. Soc.*, 2013, **135**, 1167–1176.
2 M. Armand and J.-M. Tarascon, *nature*, 2008, **451**, 652–657.
3 S. S. Zhang, *J. Power Sources*, 2006, **162**, 1379–1394.
4 K. Xu, *Chem. Rev.*, 2014, **114**, 11503–11618.
5 Y. Yamada and A. Yamada, *J. Electrochem. Soc.*, 2015, **162**, A2406.
6 Y. Yamada, J. Wang, S. Ko, E. Watanabe and A. Yamada, *Nat. Energy*, 2019, **4**, 269–280.
7 H. K. Bergstrom and B. D. McCloskey, *ACS Energy Lett.*, 2024, **9**, 373–380.
8 K. Xu, *Chem. Rev.*, 2004, **104**, 4303–4418.
9 T. Sou and C. A. Bergström, *Drug Discovery Today: Technol.*, 2018, **27**, 11–19.
10 Y. Liang, H. Job, R. Feng, F. Parks, A. Hollas, X. Zhang, M. Bowden, J. Noh, V. Murugesan and W. Wang, *Cell Rep. Phys. Sci.*, 2023, **4**, 101633.
11 D. Reber, Z. Wang, K. Amini, Y. Jing, J. Lorenzetti, K. Xu, A. Khetan and Q. Wang, *Chem. Rev.*, 2025, **125**, 11216–11259.
12 S. Lo, S. G. Baird, J. Schrier, B. Blaiszik, N. Carson, I. Foster, A. Aguilar-Granda, S. V. Kalinin, B. Maruyama, M. Politi, *et al.*, *Digital Discovery*, 2024, **3**, 842–868.
13 S. S. Datta, I. Battiato, M. A. Fernø, R. Juanes, S. Parsa, V. Prigiobbe, E. Santanach-Carreras, W. Song, S. L. Biswal and D. Sinton, *Lab Chip*, 2023, **23**, 1358–1375.

14 R. J. Hickman, M. Sim, S. Pablo-García, G. Tom, I. Woolhouse, H. Hao, Z. Bao, P. Bannigan, C. Allen, M. Aldeghi, *et al.*, *Digital Discovery*, 2025, **4**, 1006–1029.

15 N. Yoshikawa, Y. Asano, D. N. Futaba, K. Harada, T. Hitosugi, G. N. Kanda, S. Matsuda, Y. Nagata, K. Nagato, M. Naito, *et al.*, *Digital Discovery*, 2025, **4**, 1384–1403.

16 L. Roberts, M. E. Reish, J. Yang, W. Zhang, J. S. Derasp and J. E. Hein, *Digital Discovery*, 2025, **4**, 979–986.

17 N. Yoshikawa, K. Darvish, M. G. Vakili, A. Garg and A. Aspuru-Guzik, *Digital Discovery*, 2023, **2**, 1745–1751.

18 M. B. Rooney, B. P. MacLeod, R. Oldford, Z. J. Thompson, K. L. White, J. Tungjunyatham, B. J. Stankiewicz and C. P. Berlinguette, *Digital Discovery*, 2022, **1**, 382–389.

19 J. T. Yik, L. Zhang, J. Sjölund, X. Hou, P. H. Svensson, K. Edström and E. J. Berg, *Digital Discovery*, 2023, **2**, 799–808.

20 I. Oh, M. A. Pence, N. G. Lukhanin, O. Rodríguez, C. M. Schroeder and J. Rodríguez-López, *Device*, 2023, **1**, year.

21 B. P. MacLeod, F. G. Parlane, T. D. Morrissey, F. Häse, L. M. Roch, K. E. Dettelbach, R. Moreira, L. P. Yunker, M. B. Rooney, J. R. Deeth, *et al.*, *Sci. Adv.*, 2020, **6**, eaaz8867.

22 N. Fisker-Bødker, D. Persaud, Y. Bai, M. Kozdras, T. Vegge, J. Hattrick-Simpers and J. H. Chang, *Digital Discovery*, 2025.

23 A. Dave, J. Mitchell, S. Burke, H. Lin, J. Whitacre and V. Viswanathan, *Nat. Commun.*, 2022, **13**, 5454.

24 N. Xin, Y. Sun, M. He, C. J. Radke and J. M. Prausnitz, *Fluid Phase Equilib.*, 2018, **461**, 1–7.

25 D. Schaefer and M. Kohns, *Fluid Phase Equilib.*, 2023, **571**, 113802.

26 S. Black, L. Dang, C. Liu and H. Wei, *Org. Process Res. Dev.*, 2013, **17**, 486–492.

27 J. A. Selekman, J. Qiu, K. Tran, J. Stevens, V. Rosso, E. Simmons, Y. Xiao and J. Janey, *Annu. Rev. Chem. Biomol. Eng.*, 2017, **8**, 525–547.

28 B. Hoelke, S. Gieringer, M. Arlt and C. Saal, *Anal. Chem.*, 2009, **81**, 3165–3172.

29 P. Shiri, V. Lai, T. Zepel, D. Griffin, J. Reifman, S. Clark, S. Grunert, L. P. Yunker, S. Steiner, H. Situ, *et al.*, *Iscience*, 2021, **24**, year.

30 M. N. Bahr, D. B. Damon, S. D. Yates, A. S. Chin, J. D. Christopher, S. Cromer, N. Perrotto, J. Quiroz and V. Rosso, *Org. Process Res. Dev.*, 2018, **22**, 1500–1508.

31 N. P. Tu and B. J. Kotecki, *The Power of High-Throughput Experimentation: General Topics and Enabling Technologies for Synthesis and Catalysis (Volume 1)*, American Chemical Society, 2022, vol. 1419, ch. 11, pp. 189–202.

32 S. Doloi, M. Das, Y. Li, Z. H. Cho, X. Xiao, J. V. Hanna, M. Osvaldo and L. N. W. Tat, *Digital Discovery*, 2025, **4**, 1685–1721.

33 J. Redmon, J. Redmon, S. Divvala, S. K. Divvala, R. Girshick, R. Girshick, A. Farhadi and A. Farhadi, *Computer Vision and Pattern Recognition*, 2016.

34 Y. Jiang, H. Fakhruldeen, G. Pizzuto, L. Longley, A. He, T. Dai, R. Clowes, N. Rankin and A. I. Cooper, *Digital Discovery*, 2023, **2**, 1733–1744.

35 Y. Chen, H. Lin, T. Zhang, A. Dave, J. Mitchell, J. Whitacre and V. Viswanathan, *SoftwareX*, 2026, **34**, 102565.

36 K. J. Oguine, O. C. Oguine and H. I. Bisallah, *5th In-formation Technology for Education and Development (ITED)*, 2022.

37 NaNO3 PubChem page, https://pubchem.ncbi.nlm.nih.gov/compound/Sodium-Nitrate, Accessed August 20, 2025.

38 Li2SO4 Chemical Book page, https://www.chemicalbook.com/ChemicalProductProperty_EN_CB3408669.htm, Accessed August 20, 2025.